One difficulty remains, namely, the singularity that occurs when $y=y'$. It is the Hankel function $H_0^{(2)}(k_0|y-y'|)$ that contains the singularity. The procedure used is as follows. In the vicinity of $y=y'$, the Hankel function is replaced by its small argument form which is integrable, and its average value over the interval is taken. This procedure yields

$$\overline{H_0^{(2)}(k_0|y-y'|)} \approx 1 - j\frac{2}{\pi}\left\{\ln\frac{\gamma}{2} - 1 + \ln\frac{\Delta}{2}\right\} \tag{11}$$

in which γ is Euler's constant and the bar represents "the average value of." The unknown current distribution can now be determined by the inversion of (10). Whenever $i=j$, (11) is used instead of the Hankel function. The Gauss–Jordon technique was used to solve this system of equations.

IV. Results

The parameters of the surface-wave system used for the computation and experiment are: the thickness of the dielectric, $k_0t=0.312$; attenuation constant, $(\alpha_0/k_0)=0.188$; and the dielectric constant, $\kappa=2.54$. The experimental apparatus was designed to operate at 9.375 GHz. Typical computed and measured values of the magnitude and phase angle of the reflection coefficients for strips of various widths and heights above the surface-wave system are displayed graphically in Figs. 2–3. The experimental values were obtained from measurements made with the use of the apparatus described in detail in [3].

An examination of the computed values shown in Fig. 2 reveals, not surprisingly, that for a given strip width the closer the strip is to the dielectric surface the more increments that are required for the numerical solution. For example, notice that for $k_0h=2.51$ and $k_0h=5.02$ the strip was divided into 70 increments. Excellent correspondence between calculated and measured values for strip widths over the full range of values considered was obtained when $k_0h=5.02$. Note, however, that when the height is lowered to $k_0h=2.51$ a significant deviation from the experimental values is noted when $k_0w>13.5$. Although not shown, the calculated data began to deviate from the measured data for $k_0h=0.5$ when k_0w was only equal to 3. When N was increased to 150 the correspondence was good up to $k_0w=8$, as can be seen from Fig. 2. Even so, in the latter case the deviation from the experiment is only eight percent for widths up to $k_0w=15$.

The transmission coefficient can be computed with the use of (3). The results are shown in Figs. 4 and 5. The normalized impedance is computed with the use of (4). These results are shown in Fig. 6. Note that the real part of the impedance for each case considered remains very nearly constant as the strip width is varied. Furthermore, once the width reaches a certain value the impedance stays fairly constant thereafter, with the impedance curve forming loops about a constant value. Also, the impedance is always capacitive as one might expect.

The computed fractions of power reflected, radiated, and transmitted are displayed in Figs. 7–9. Notice that as a strip of a given width is moved away from the surface, that is, as k_0h increases, the fraction of reflected power decreases and that of the transmitted power increases, both in a seemingly monotonic fashion. The fraction of radiated power, on the other hand, first increases then decreases, giving rise to a pronounced maximum at a critical height. This was investigated by computing the fraction of power radiated as a function of height with the width as a parameter. The results are shown in Fig. 10. Sketched in that figure is the locus of the maxima. Note that for narrow strips the maxima occur at a height very nearly one-half wavelength, whereas for wide strips the maxima occur at heights that are closer to one-quarter wavelength. Note the smooth transition in the heights where the maxima occur as the strip widths vary from narrow to wide.

Another striking feature of the results is that the maxima never exceed 0.5, although they do tend to approach that value for wider strips. While no formal proof is given it does appear that the maximum fraction of radiated power of a conducting strip might be 0.5.

Acknowledgment

The authors wish to thank V. P. Cable for making the measurements presented herein.

References

[1] R. S. Elliott and E. N. Rodda, "Parasitic arrays excited by surface waves," *IRE Trans. Antennas Propagat.*, vol. AP-3, pp. 140–142, July 1955.
[2] J. W. Duncan and R. H. DuHamel, "A technique for controlling the radiation from dielectric rod waveguides," *IEEE Trans. Antennas Propagat.*, vol. AP-5, pp. 284–289, July 1957.
[3] E. S. Gillespie and J. J. Gustincic, "The scattering of a TM surface wave by a perfectly conducting strip," *IEEE Trans. Microwave Theory Tech. (Special Issue on Microwave Filters)*, vol. MTT-13, pp. 630–640, Sept. 1965.
[4] ——, "The scattering of an axial cylindrical surface wave by a perfectly conducting plane annulus," *IEEE Trans. Microwave Theory Tech.*, vol. MTT-16, pp. 334–341, June 1968.
[5] E. S. Gillespie, "The impedance and scattering properties of a plane annulus surrounding a Goubau line," *IEEE Trans. Microwave Theory Tech.* (Corresp.), vol. MTT-19, pp. 837–839, Oct. 1971.
[6] E. S. Gillespie and J. J. Gustincic, "The scattering of a plane wave by a perfectly conducting strip," Dep. Eng., Univ. of California, Los Angeles, Rep. 64-56, 1964.
[7] F. J. Kilburg, "The impedance and scattering properties of a perfectly conducting strip above a plane surface wave system," Master's thesis, California State Univ., Northridge, 1972.

Experimental Gain and Noise Parameters of Microwave GaAs FET's in the *L* and *S* Bands

A. Anastassiou and M. J. O. Strutt

***Abstract*—The design of microwave amplifiers with GaAs FET's assumes the knowledge of the four gain and the four noise parameters as a function of the biasing conditions. The gain parameters at three different bias conditions have been calculated by computer from the measured scattering parameters. The noise figures as a function of the same bias conditions have also been measured. The four fundamental noise parameters have been determined. The GaAs FET's are units from Plessey (England). At present, these are the only units which are commercially available.**

I. Gain Parameters

The available gain of a two-port as a function of the four gain parameters is given by

$$\frac{1}{G_{av}} = \frac{1}{G_{avo}} + \frac{Q_g}{1 - U_s^2 - V_s^2}\left[(U_s - U_{og})^2 + (V_s - V_{og})^2\right] \tag{1}$$

where G_{avo} is the maximum available gain of the two-port, $r_{og}=U_{og}+jV_{og}$ the optimum complex source reflection coefficient with respect to gain, Q_g a factor which indicates the dependence of the available gain on the complex source reflection coefficient, and $r_s=U_s+jV_s$ the complex reflection coefficient of the source.

The four gain parameters as a function of the scattering parameters, which are determined in [2], are given by

$$G_{avo} = \frac{|s_{21}|}{|s_{12}|}\cdot(K - \sqrt{K^2-1}) \tag{2}$$

$$Q_g = \frac{1}{G_{avo}} + \frac{|s_{11}|^2 - |\Delta|^2}{|s_{21}|^2}, \qquad \Delta = s_{11}s_{22} - s_{21}s_{12} \tag{3}$$

$$U_{og} = \frac{\mathrm{Re}\,(C)}{|s_{21}|^2\cdot Q_g}, \qquad C = s_{11} = s_{22}^*\,\Delta \tag{4}$$

$$V_{og} = \frac{-\mathrm{Im}\,(C)}{|s_{21}|^2\cdot Q_g}. \tag{5}$$

Here, K is the stability factor. If $K>1$, the two-port is unconditionally stable and the gain parameters are given by (2)–(5). If $K<1$, the two-port is conditionally stable and the available gain becomes equal to the maximum stable gain (MSG):

$$\mathrm{MSG} = \frac{|s_{21}|}{|s_{12}|}. \tag{6}$$

Manuscript received August 14, 1972; revised November 13, 1972. This work was supported by the Swiss National Foundation for the Promotion of Scientific Research.

The authors are with the Department of Advanced Electrical Engineering, Swiss Federal Institute of Technology, 8006 Zurich, Switzerland.

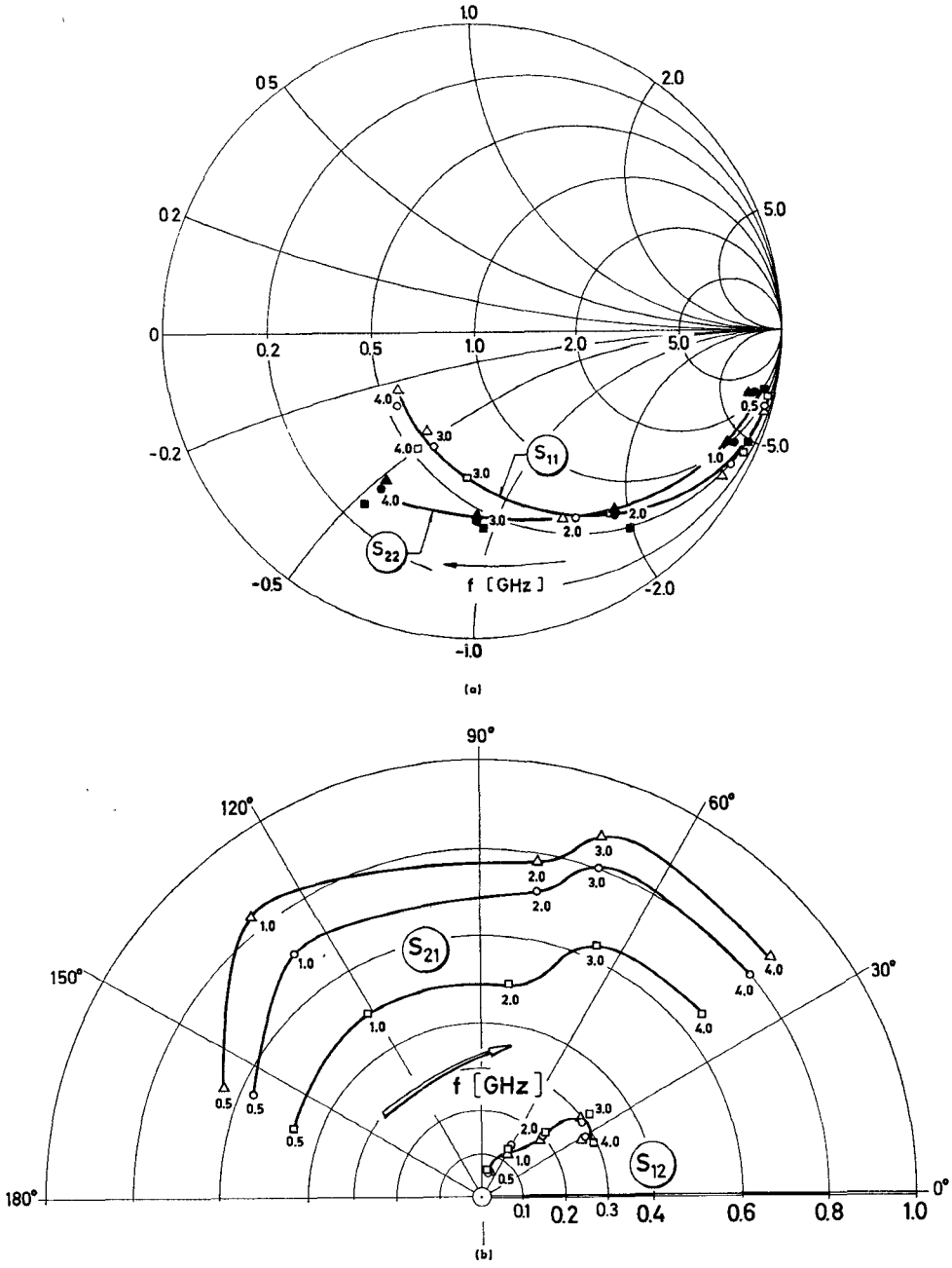

Fig. 1. Scattering parameters as a function of frequency. □: $U_D=4$ V, $I_D=2$ mA; ○: $U_D=4$ V, $I_D=5$ mA; △: $U_D=4$ V, $I_D=8$ mA. (a) s_{11} and s_{22} parameter. (b) s_{12} and s_{21} parameter.

The scattering parameters of a GaAs FET with a gate electrode of the Schottky-barrier type have been measured using a network analyzer (Hewlett-Packard). Fig. 1 shows the four scattering parameters as a function of the frequency f. In Fig. 2 the maximum available gain and the factor Q_g for several bias conditions are represented. In the frequency region between 0.5 and 2 GHz the transistor is conditionally stable and the available gain becomes equal to the MSG.

In the frequency region between 2 and 4 GHz the transistor is unconditionally stable. Thus the factors Q_g and r_{og} can only be defined in the second frequency region. Fig. 3 shows circles of constant available gain plotted on a source admittance plane.

II. Noise Parameters

The noise figure of a two-port as a function of the noise parameters is given by

$$F = F_{\min} + \frac{R_n}{G_s}\left[(G_s - G_{on})^2 + (B_s - B_{on})^2\right] \tag{7}$$

where F is the noise figure of the two-port corresponding to the source admittance $Y_s=G_s+jB_s$, $F_{\min}$ is the minimum noise figure, R_n the noise resistance, and $Y_{on}=G_{on}+jB_{on}$ the optimum source admittance with respect to the noise figure.

The noise figure of the same transistor type has been measured. Fig. 4 shows the minimum noise figure $F_{\min}$ as a function of the frequency for three different drain currents. Fig. 5 represents the complex-conjugate value of s_{11}, the optimum reflection coefficient with respect to gain $r_{og}(Y_{og})$, and the optimum source impedance $Z_{on}=1/Y_{on}$ with respect to noise [5], [6]. Fig. 5 allows a useful comparison between the above three parameters in view of an optimum application in an amplifier circuit. Fig. 6 shows the noise resistance as a function of frequency.

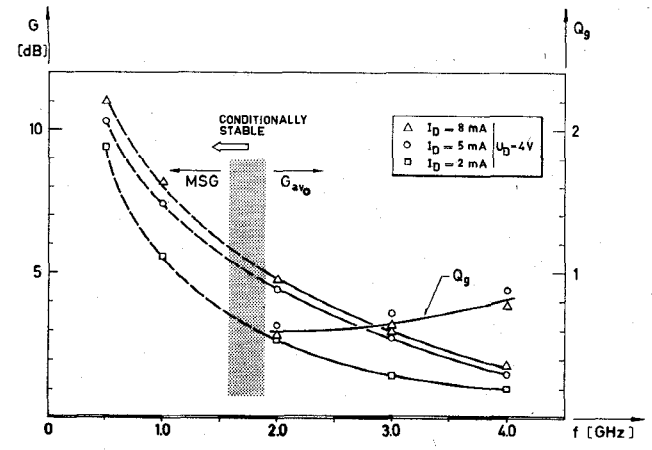

Fig. 2. Maximum available gain G_{av_0}, MSG, and Q_g factor as a function of frequency. □: U_D = 4 V, I_D = 2 mA; ○: U_D = 4 V, I_D = 5 mA; △: U_D = 4 V, I_D = 8 mA.

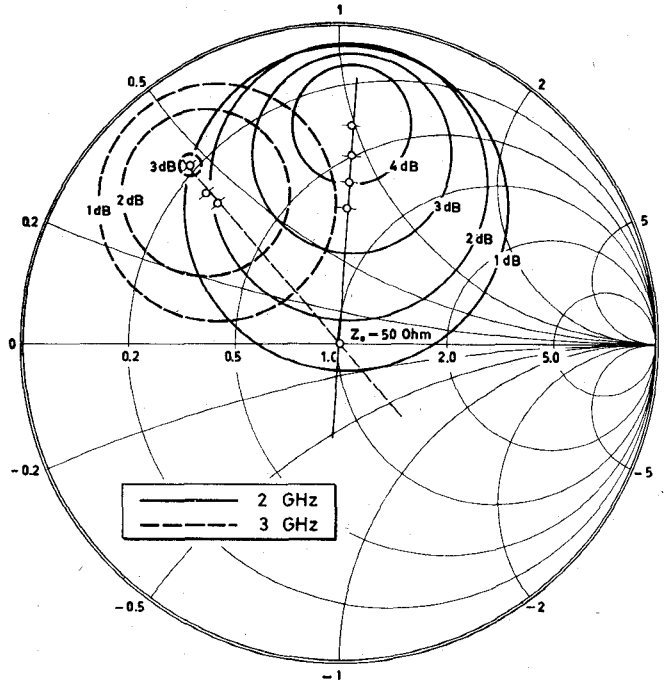

Fig. 3. Circles of constant available gain: U_D = 4 V, I_D = 8 mA.

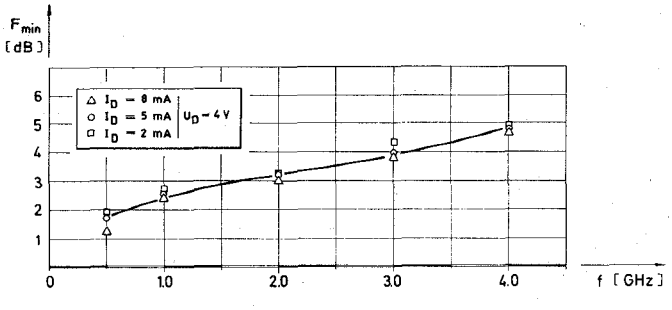

Fig. 4. Minimum noise figure F_{min} as a function of frequency. □: U_D = 4 V, I_D = 2 mA; ○: U_D = 4 V, I_D = 5 mA; △: U_D = 4 V, I_D = 8 mA.

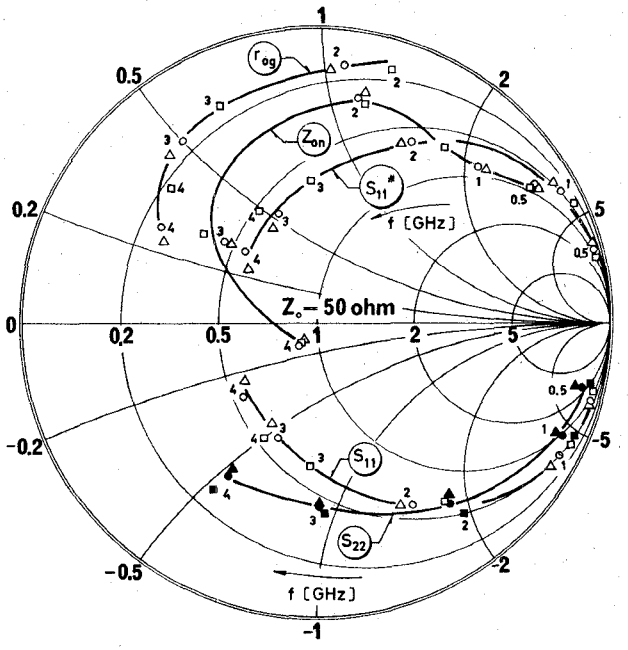

Fig. 5. Optimum source reflection coefficient r_{og} with respect to gain; optimum source impedance with respect to noise Z_{on}; complex conjugate of s_{11} parameter, (s_{11}^*), s_{11}, and s_{22} parameters. □: U_D = 4 V, I_D = 2 mA; ○: U_D = 4 V, I_D = 5 mA; △: U_D = 4 V, I_D = 8 mA.

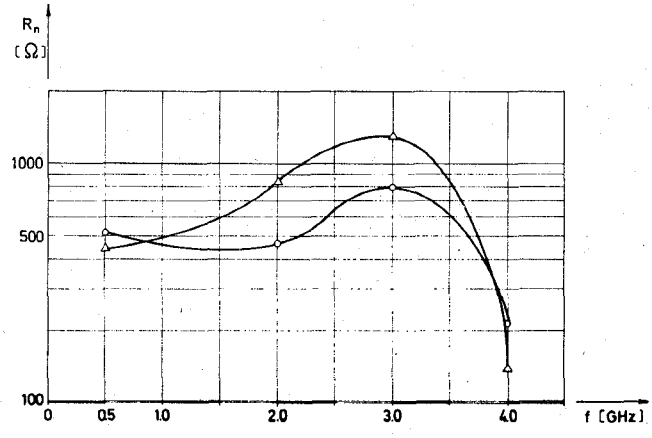

Fig. 6. Noise resistance as a function of frequency. ○: U_D = 4 V, I_D = 5 mA; △: U_D = 4 V, I_D = 8 mA.

III. Conclusions

For an adequate application in a microwave amplifier circuit, the knowledge of the gain and noise behavior of the device is essential. The knowledge of the gain behavior given by the four gain parameters G_{av_0}, Q_g, U_{og}, and V_{og} and the knowledge of the noise behavior given by the noise parameters F_{min}, R_n, G_{on}, and B_{on} are therefore indispensable.

References

[1] G. E. Bodway, "Two-port flow analysis using generalized scattering parameters," *Microwave J.*, vol. 10, pp. 61–69, May 1967.
[2] K. Hartmann, W. Kotyczka, and M. J. O. Strutt, "Experimental gain parameters of three microwave-bipolar transistors in the 2- to 8-GHz range," *Proc. IEEE* (Corresp.), vol. 59, pp. 1720–1721, Dec. 1971.
[3] "IRE standards on methods of measuring noise in linear twoports, 1959," *Proc. IRE*, vol. 48, pp. 60–68, Jan. 1960.
[4] W. Baechtold and M. J. O. Strutt, "Noise in microwave transistors," *IEEE Trans. Microwave Theory Tech. (Special Issue on Noise)*, vol. MTT-16, pp. 578–585, Sept. 1968.

[5] A. Leupp and M. J. O. Strutt, "Noise behaviour of the MOSFET at VHF and UHF," *Electron. Lett.*, vol. 4, no. 15, July 1968.
[6] ——, "High-frequency FET noise parameters and approximation of the optimum source admittance," *IEEE Trans. Electron Devices*, vol. ED-16, pp. 428–431, May 1969.

State-Space Analysis of a Magnetically Tuned IMPATT Oscillator Lumped Model

I. J. H. S. MOORE AND J. A. C. STEWART

I. Introduction

One method of frequency modulating an IMPATT-diode oscillator uses a ferrite whose susceptibility is a function of applied dc magnetic field. Octave band tuning of Gunn oscillators using yttrium iron garnet (YIG) has been reported by several authors [1], [2]. The YIG comprised the principal energy-storage element apart from the active device. For applications requiring relatively small frequency deviations (500 MHz), a YIG sphere can be used to perturb the resonant frequency of the oscillator cavity, and hence to vary the oscillation frequency. This short paper describes the derivation and analysis of a lumped model of the YIG tuned cavity IMPATT oscillator.

While a large-signal time-domain solution of the equations resulting from the lumped model has been obtained, the computer time required for a steady-state solution is prohibitive. In addition, the complex microwave circuit can support frequencies which are not harmonically related, which makes it difficult to interpret the large-signal waveforms in terms of frequency components. By using the small-signal form of the diode lumped model equations, the complex natural frequencies for the complete system can be evaluated for given values of dc magnetic field [3]. Comparison of computed and experimental oscillator tuning results indicates that the small-signal IMPATT-diode model should be modified to account for large-signal effects. The modified oscillator model shows good agreement with experimental results, and hence may be used as a tool to investigate further the oscillator tuning behavior.

In the analysis, the YIG tuned oscillator is subdivided into three distinct regions: the IMPATT-diode chip, the microwave circuit external to the chip and YIG sphere, and the YIG tuning sphere. By sectioning the oscillator components in this manner, it is possible to use this approach to analyze many differing oscillator configurations. The derivation of lumped models for these separate regions is described in Sections II–IV, respectively. State-space analysis of the complete oscillator lumped model is discussed in Section V. Section VI indicates the large-signal modifications to the small-signal diode lumped model. The validity of the model, in comparison with experimental measurements, is demonstrated in Section VII.

II. IMPATT-Diode Lumped Model

A small-signal lumped model of an IMPATT diode exists, which includes realistic hole and electron ionization rates and saturation velocities [3]. The model is accurate for p-i-n type structures, but becomes less accurate for diodes with more localized avalanche regions. A uniform avalanche region dc electric field is assumed, equal to the maximum dc electric field in the depletion region. The avalanche region width is found using the ionization integral for this p-i-n diode approximation. Fig. 1(b), which indicates the ionization rate for electrons, α_n for a n^+-p-p^+ diode demonstrates the inadequacy of the uniform electric field approximation. In the present model, therefore, the ionization-rate curves are approximated by a series of steps, as shown in the figure.

Solution of the steady-state continuity equations for holes and electrons, and Poisson's equation, yields, for a given bias current, the electric field and hole and electron current profiles in the diode depletion layer [Fig. 1(a)]. In order to speed up the computation, the

Manuscript received August 15, 1972; revised December 8, 1972. This work was supported by the Science Research Council, England.
The authors are with the Department of Electrical and Electronic Engineering, Ashby Institute, Queen's University, Belfast, Northern Ireland.

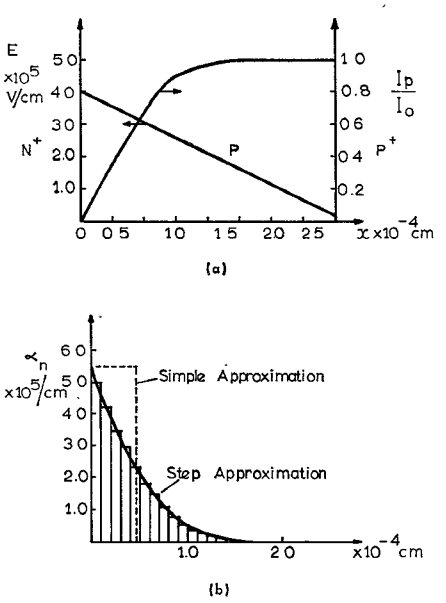

Fig. 1. (a) Static electric field and hole current profiles in n^+-p-p^+ diode depletion layer. (b) Electron ionization rate approximations in n^+-p-p^+ diode depletion layer.

avalanche region width is defined as the distance from the junction at which the hole current reaches 98 percent of its final value. The average dc electric fields in the avalanche lumps are perturbed until the ionization integrals approach unity to within a specified tolerance. The values of α_n and α_p are then computed for each lump and used to evaluate the small-signal diode behavior [3]. Fig. 2 contrasts the diode small-signal impedance at a dc bias current of 20 mA computed 1) using the simple small-signal model, 2) using the modified small-signal model, and 3) using a model which evaluates the large-signal diode impedance as a function of RF applied voltage. The curve is obtained for low values of RF applied voltage. The modified small-signal model is seen to be consistent with the large-signal model over the normal diode operating frequency range, while requiring only a fraction of the computer time. The diode parameters are: cross-sectional area $=0.9\times10^{-4}$ cm^2, depletion layer width $=2.7\times10^{-4}$ cm, epitaxial layer doping density $=0.9\times10^{16}$ cm^{-3}, saturated electron velocity $=8.5\times10^6$ cm$\cdot$s^{-1}, and saturated hole velocity $=7.0\times10^6$ cm$\cdot$s^{-1}.

The state variables used to describe the diode behavior are the small-signal electric fields at the lump edges and the total small-signal hole charges in the lump. The model results in a set of state equations. The variables used to couple the diode to the external circuit are the small-signal diode voltage and current.

III. Microwave External Circuit Model

The external microwave circuit is separated into two regions: a uniform transmission-line region, which in this study may consist of a coaxial-line or a radial-line section, and the diode pill encapsulation and mount.

The uniform line may be described by a ladder network of lumped elements. For a reasonably accurate representation, each section of the ladder network should be equivalent to a line length less than $\lambda/15$, where λ is the operating wavelength. The lumped-element values are determined from the capacitance and inductance per unit length of the transmission line in question. This uniform-line equivalent circuit includes the cavity coupling capacitor and load resistance.

At the microwave frequencies considered in this paper, a simple two-element equivalent circuit for the diode pill encapsulation may be used. Losses in the encapsulation and diode series resistance are included in the resistance R_s. Following Getsinger [4], the diode mount, consisting of the transforming section between the pill outer circumference and the uniform line, may be characterized by lumped elements. A modified form of Getsinger's fringing capacitances is used to more precisely describe the mount.

The lumped-element equivalent circuit for the microwave external circuit consists of a ladder network of series inductances and shunt capacitances. By defining the state variables as the inductor currents